Enhanced learning and sensory salience in a cerebellar mouse autism model

Marlies Oostland[1,†,*], Mikhail Kislin[1], Yuhang Chen[1], Tiffany Chen[2],

Sarah Jo Venditto[1], Ben Deverett[3], Samuel S.-H. Wang[1,*]

[1]Neuroscience Institute, Princeton University, Princeton, NJ, USA.

[2]Department of Neurological Surgery, University of California, San Francisco, CA, USA.

[3]Department of Anesthesiology, Stanford University Medical Center, Stanford, CA, USA.

*Corresponding authors: sswang@princeton.edu (SW), m.oostland@ucl.ac.uk (MO)

[†]Present address: Wolfson Institute for Biomedical Research, University College London, London, UK.

Among the impairments manifested by autism spectrum disorder (ASD) are sometimes islands of enhanced function[1,2]. Although neuronal mechanisms for enhanced functions in ASD are unknown, the cerebellum is a major site of developmental alteration, and early-life perturbation to it leads to ASD with higher likelihood than any other brain region[3,4]. Here we report that a cerebellum-specific transgenic mouse model of ASD shows faster learning on a sensory evidence-accumulation task[5]. In addition, transgenic mice showed enhanced sensitivity to touch and auditory cues, and prolonged electrophysiological responses in Purkinje-cell complex spikes and associative neocortical regions. These findings were replicated by pairing cues with optogenetic stimulation of Purkinje cells. Computational latent-state analysis of behavior[6–8] revealed that both groups of mice with cerebellar perturbations exhibited enhanced focus on current rather than past information, consistent with a role for the cerebellum in retaining information in memory[9]. We conclude that cerebellar perturbation can activate neocortex via complex spike activity and reduce reliance on prior experience, consistent with a weak-central-coherence account in which ASD traits arise from enhanced detail-oriented processing[1]. This recasts ASD not so much as a disorder but as a variation that, in particular niches, can be adaptive.

Autism spectrum disorder (ASD) is associated not only with deficits, but also islands of enhanced function, including perceptual domains and technical or even artistic capacities[1,2]. According to the weak central coherence account of ASD, these enhanced capacities can be explained by a detail-focused cognitive style in which individual perceptual features are emphasized. ASD is also associated with abnormality of the cerebellum, whose roles extend beyond movement to include cognition, sensory processing, learning, and memory[10–12]. Functional

effects can arise developmentally, since early-life cerebellar injury leads to ASD and other disabilities with higher likelihood than adult injury[3,4,13,14]. These nonmotor influences of the cerebellum may be conveyed via long-range connections that project throughout thalamus and neocortex[15].

Cerebellum-dependent losses of function

In mice, cerebellar disruption can lead to deficits in attention, behavioral flexibility, and social interaction[16]. However, how enhanced function emerges from abnormal cerebellar circuits is unknown. To answer this question, we examined *L7-Tsc1* mutants, a mouse model of ASD in which *tuberous sclerosis complex 1* is deleted specifically in cerebellar Purkinje cells[17,18]. *L7-Tsc1* mutant mice show perseveration and deficits in gait and social interactions (Fig. 1a), as well as deficits in relatively simple learned tasks such as delayed eyeblink conditioning and motor learning on the accelerating rotarod[17,18]. *L7-Tsc1* mutant mice have reduced numbers of Purkinje cells (Fig. 1a), and surviving Purkinje cells show lower firing rates both *ex vivo*[17] and *in vivo*, with reduced simple-spike and complex-spike rates in awake animals (Fig. 1b).

We examined more complex forms of learning and information processing by training mice to integrate sensory evidence in working memory using an established evidence-accumulation decision-making paradigm[5,20]. Post-learning performance of this task depends on cerebellar crus I[5,9], a region that is also necessary for other nonmotor functions[16], and where *L7-Tsc1* mutants have reductions in Purkinje cells (Extended Data Fig. 1). During the task, mice receive sensory air puffs on the left and right whiskers, and receive a reward for correctly licking in the direction of more puffs (Fig. 1c). Mice progress through increasingly difficult levels of task shaping during

which evidence becomes more complex and an increasing temporal delay separates sensory information from the decision (Extended Data Table 1).

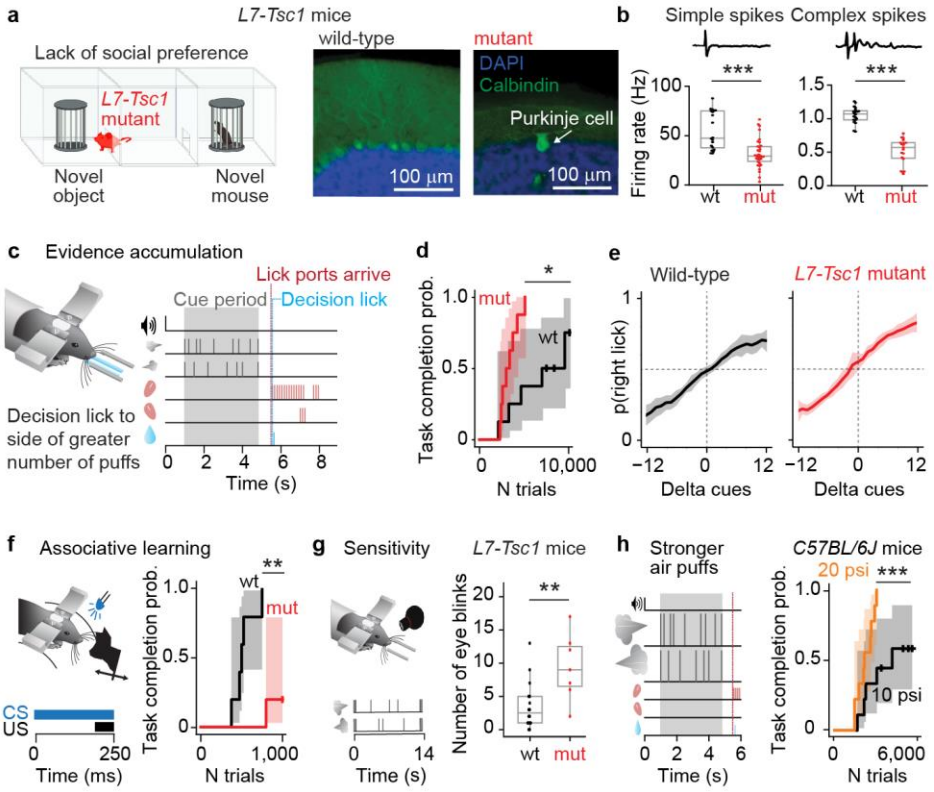

Fig. 1 | Cerebellar-impaired mice show enhanced learning of an evidence-accumulation decision-making task. a, *L7-Tsc1* mutant mice have impaired social capacity and flexible behavior[17–19] (left) and reduced number of Purkinje cells in the cerebellar cortex (right). **b,** Reduced spontaneous *in vivo* firing rates of simple spikes and complex spikes in *L7-Tsc1* mutant mice (simple spikes: n = 34 cells, mean = 32 Hz, complex spikes: n = 19 cells from 4 mice, mean = 0.51 Hz) compared to wild-type littermates (simple spikes: n = 20 cells, mean = 55 Hz, $t(1) = 5.06$, $P = 5.5 \times 10^{-6}$, complex spikes: n = 20 cells from 5 mice, mean = 1.05 Hz, $t(1) = 10.55$, $P = 1.1 \times 10^{-12}$, both two-sided Student's t-tests). The duration of the example waveforms above each plot is 15 ms. **c,** The evidence-accumulation task. Mice receive sensory air puffs on the left and right whiskers, and receive a reward for correctly licking in the direction of more puffs. **d,** Kaplan-Meier estimator of probability of reaching the final level of task training for *L7-Tsc1* mutant mice (n = 8, median 3410 trials) and wild-type littermates (n = 8, median 9636 trials, $\chi^2(1) = 6.49$, $P = 0.011$, log-rank test). **e,** Psychometric performance curves in mice who recently reached the final level show no change in bias ($t(1) = 1.73$, $P = 0.21$), slope ($t(1) = 0.15$, $P = 0.70$), or lapse rate ($t(1) = 3.44$, $P = 0.085$, all two-sided Student's t-tests). Shading represents 1 s.d. **f,** Impaired learning of the delayed tactile startle conditioning task for *L7-Tsc1* mutant mice (n = 5, median 1000 trials) compared to wild-type littermates (n = 5, median 500

trials, $\chi^2(1) = 9.70$, $P = 0.0018$, log-rank test). **g,** Increased sensory sensitivity in *L7-Tsc1* mutant mice ($n = 16$) compared to wild-type littermates ($n = 7$, $t(1) = 10.30$, $P = 0.0042$, two-sided Student's *t*-test unadjusted; for full data set see Extended Data Fig. 2). **h,** Increased sensory salience through stronger puffs also leads to enhanced learning. Kaplan-Meier estimator of task completion for *C57BL/6J* animals receiving standard (10 psi, $n = 9$, median 4275 trials) or stronger (20 psi, $n = 9$, median 2225 trials) whisker puffs during the evidence accumulation task ($\chi^2(1) = 7.11$ $P = 0.00047$, log-rank test). Shaded areas in Kaplan-Meier curves represent 95% confidence intervals.

Enhanced learning and sensory responses

L7-Tsc1 mutant mice successfully reached the final level of training twice as quickly as wild-type littermates (Fig. 1d), showing enhanced learning capabilities. The faster learning rate was not correlated with age or corticosterone level. Faster learning already occurred at the earliest stages of training (Extended Data Fig. 8). Once animals had reached the expert stage, in the first few sessions at the final level there was no difference in overall performance between *L7-Tsc1* mutant mice and their wild-type littermates (Fig. 1e). This performance is comparable to animals who have been trained extensively at the final level of a similar task[5,9,20]. Despite their accelerated learning on the air puff task, *L7-Tsc1* mutant mice were still slower to learn a separate delay tactile startle conditioning behavior (DTSC)[21] (Fig. 1f), a cerebellum-dependent form of classical conditioning involving simple sensory association[18].

We hypothesized that the superior learning rate in these mice might be related to sensory processing of air puffs. Because effects on learning rate were already present from the onset, we measured sensory sensitivity before training on the evidence-accumulation task. Naive *L7-Tsc1* mutant mice showed enhanced response to individual air puffs (Fig. 1g with full dataset in Extended Data Fig. 2b), as well as to auditory stimuli (Extended Data Fig. 2c,d), indicative of altered sensory processing. In wild-type *C57BL/6J* mice, increasing the intensity of air puffs from 10 psi to 20 psi was sufficient to accelerate training to a degree similar to that seen in *L7-Tsc1*

mutant mice (Fig. 1h). This suggests that early sensory sensitivity may aid in high-accuracy performance during learning of a task requiring integration of sensory evidence, such as the evidence-accumulation task.

To measure the neural signals accompanying enhanced learning capacity, we performed *in vivo* electrophysiological recordings in crus I in awake behaving naive mice (Fig. 2a), since improved learning was already evident at early stages of training. In wild-type mice, sensory cues triggered complex spikes (Fig. 2b), with a delayed simple-spike response (Fig. 2c). In contrast, in *L7-Tsc1* mutant mice, complex spikes were activated only after a delay of several hundred milliseconds (Fig. 2b), with decreased simple-spike response (Fig. 2c) and consequent disinhibition of negative feedback from deep nuclei (Extended Data Fig. 3a) onto inferior olivary neurons[22,23].

Deep nuclear neurons send excitatory disynaptic projections throughout neocortex[15], including two associative regions implicated in decision-making[24–26] that receive substantial disynaptic input from crus I[15]: anterior cingulate (Fig. 2d) and anterolateral motor cortex (Extended Data Fig. 3b). Recordings from these regions showed an enhancement in cue-evoked activity with a similar time course as complex-spike activity. These effects were not seen in the barrel field of the primary somatosensory cortex (Extended Data Fig. 3c). These results suggest that cerebellar neural activity might play a causal role in influencing neocortical activity to drive learning.

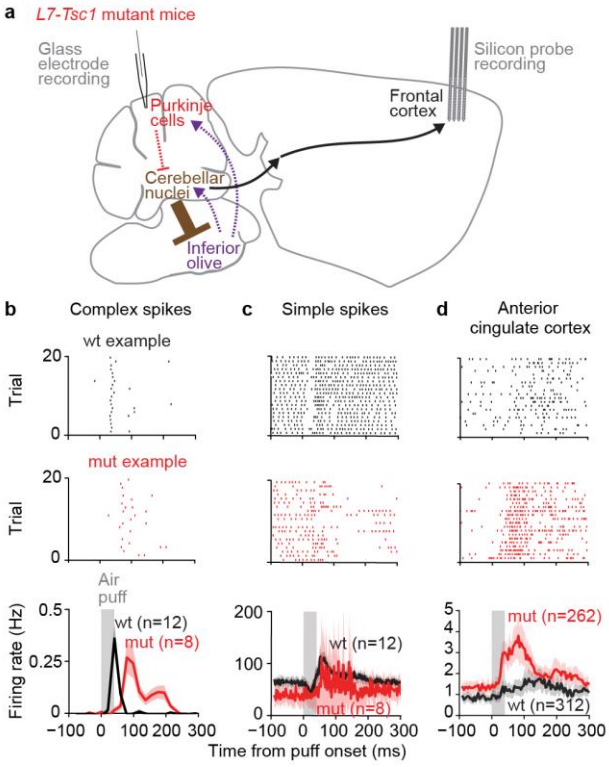

Fig. 2 | Prolonged whisker puff responses in awake behaving *L7-Tsc1* mice in cerebellar complex spikes and forebrain. a, Recording sites in cerebellum-neocortical path of influence in whisker puff responses in *L7-Tsc1* mutant mice. **b-d,** Example raster plots of Purkinje cell complex spikes (**b**), Purkinje cell simple spikes (**c**) and for anterior cingulate cortex (**d**) during 20 trials from one wild-type animal (top) and one *L7-Tsc1* mutant animal (middle), and average firing rates in response to an air puff to the whiskers (data from 4 *L7-Tsc1* mutants and 5 wild-type mice). Shaded areas represent 95% confidence intervals.

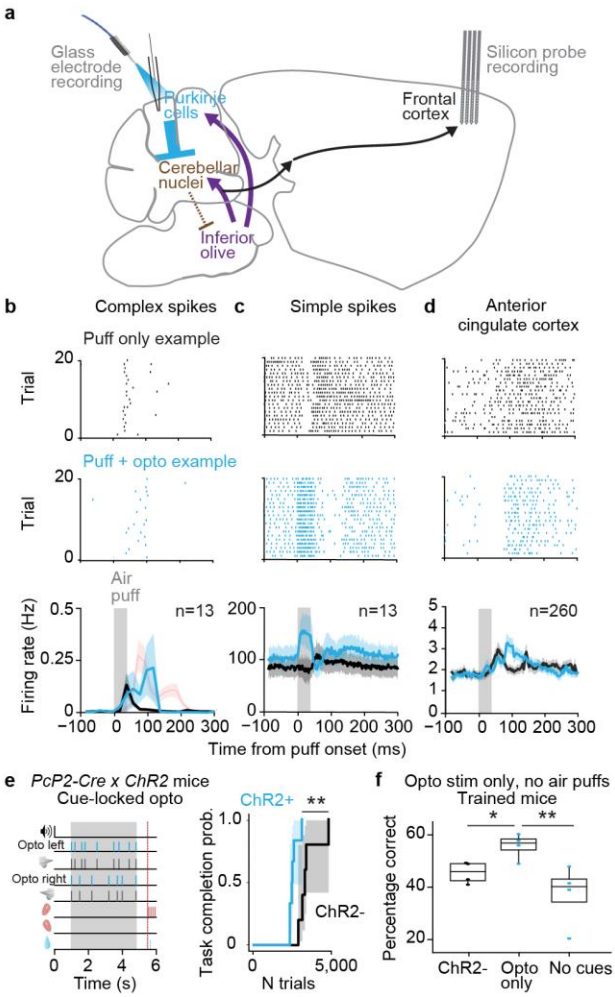

Fig. 3 | Altered whisker puff responses and faster learning with cue-locked optogenetic activation of Purkinje cells. a, Recording sites in cerebellum-neocortical path of influence in whisker puff responses paired with optogenetic stimulation of Purkinje cells in crus I. **b-d,** Example raster plots of Purkinje cell complex spikes (**b**, data from 4 mice), Purkinje cell simple spikes (**c**), and anterior cingulate cortex (**d**, data from 3 mice) during 20 trials with only a whisker puff (top) or with a whisker puff paired with optogenetic stimulation (middle), and average firing rates (bottom). The red line in the bottom plot of **b** indicates the firing rate for *L7-Tsc1* mutant mice (Fig. 2b) for comparison. Shaded areas represent 95% confidence intervals. **e,** Schematic and Kaplan-Meier estimator of task completion probability for *Pcp2-Cre* × *ChR2* mice with cue-locked bilateral optogenetic activation of crus I in the evidence-accumulation task (n = 6, median 2512 trials) and wild-type littermates (n = 5, median 3311 trials, $\chi^2(1) = 8.18$, P = 0.0042, log-rank test). **f,** Performance in the evidence-accumulation task in trained *Pcp2-Cre* × *ChR2* mice with only cue-locked optogenetic activation of Purkinje cells in crus I (n = 4, mean percentage correct: 55.8%), and two controls without stimuli: one without ChR2 expression (n = 4, 45.6% correct), the other without light (n = 4, 37.2% correct). Overall effect: $H(2) = 7.65$, P = 0.022 (Kruskal-Wallis test), with significant differences between ChR2+ and ChR2- mice (P =

0.046, Conover post-hoc test) and ChR2+ and no cues (P = 0.0044). Due to anti-biasing parameters, chance level is different for each animal but always below 50%.

Optogenetic replication of fast learning

To understand whether the neocortical activity and enhanced learning found in *L7-Tsc1* mutant mice is driven by Purkinje cell complex spikes or simple spikes, we directly manipulate simple spike activity by expressing the optogenetic probe channelrhodopsin-2 in Purkinje cells of wild-type mice. *In vivo* recordings in awake behaving naive ChR2-expressing mice (Fig. 3a) indeed showed an increase in simple spike firing during the air puff paired with optogenetic stimulation (Fig. 3c), which is the opposite effect of that seen in *L7-Tsc1* mutant mice. On the other hand, complex spike firing was increased and delayed (Fig. 3b), a similar effect to that seen in *L7-Tsc1* mutant mice, due to a putatively disinhibitory effect of simple-spike firing on nucleo-olivary paths[27]. Firing enhancement coincided with the end of the optogenetic stimulus (Extended Data Fig. 4d), consistent with a disinhibitory effect. Furthermore, silicon probe recordings in neocortex showed enhancements in associative anterior cingulate (Fig. 3d) and anterolateral motor region (Extended Data Fig. 4b) activity, but not in the barrel field of the primary somatosensory cortex (Extended Data Fig. 4c), mimicking neocortical activity in *L7-Tsc1* mutant mice. Behavioral results were consistent with the similarity in complex spike and neocortical activity patterns compared to *L7-Tsc1* mutant mice: pairing sensory stimuli with ipsilateral light flashes applied over crus I also led to faster learning than in controls not expressing ChR2 (Fig. 3e). After training, optogenetic stimuli delivered without sensory cues could also drive decision-making above chance (Fig. 3f), suggesting that alterations in Purkinje cell activity could target effectors in common with sensory cues. Thus learning can be augmented by perturbation of Purkinje cell complex-spike activity during sensory stimulation, either via Tsc1 knockout or by optogenetic

activation, both of which generate similar alterations of complex spike timing and neocortical activity.

Mutants stay on-task and in the present

To understand the relation between early sensory sensitivity and high-accuracy performance throughout training, we performed computational latent-state analysis of the learning process. This analysis identifies shifts in behavioral response patterns occurring between groups of trials that reveal variations in internal states over time[6–8]. We fitted trial-by-trial outcomes to a generalized linear model - hidden Markov model (GLM-HMM), trained on a separate data set of 22 wild-type mice and then fitted to the experimental animals (Fig. 4a).

Based on these fits, mouse behavior could be sorted into three major categories that differed in their dependence on task parameters (Fig. 4b). Mice in the on-task state 1 made the most correct decisions, relying heavily on the left-right difference in sensory cues (Fig. 4c), and less on the animals' choice in the previous trial (Fig. 4d). In all mice, learning was accompanied by more time spent in the on-task state (Fig. 4f,g,i). Early in training, wild-type mice tended to spend time in state 2, a past-trial-driven state in which mice relied more heavily on past rather than present information, thus reducing their decision accuracy (Fig. 4c), with responses strongly dependent on the choices made in the previous two trials (Fig. 4d); and state 3, an inattentive state in which mice were only weakly sensitive to any features of the task (Fig. 4c,d). On a moment-to-moment basis, wild-type mice made transitions from state to state on the time scale of dozens or hundreds of trials (Fig. 4e). Transitions away from state 1 occurred largely at the end of a session, when animals switch from the on-task state to the disengaged state (see example in Fig. 4f).

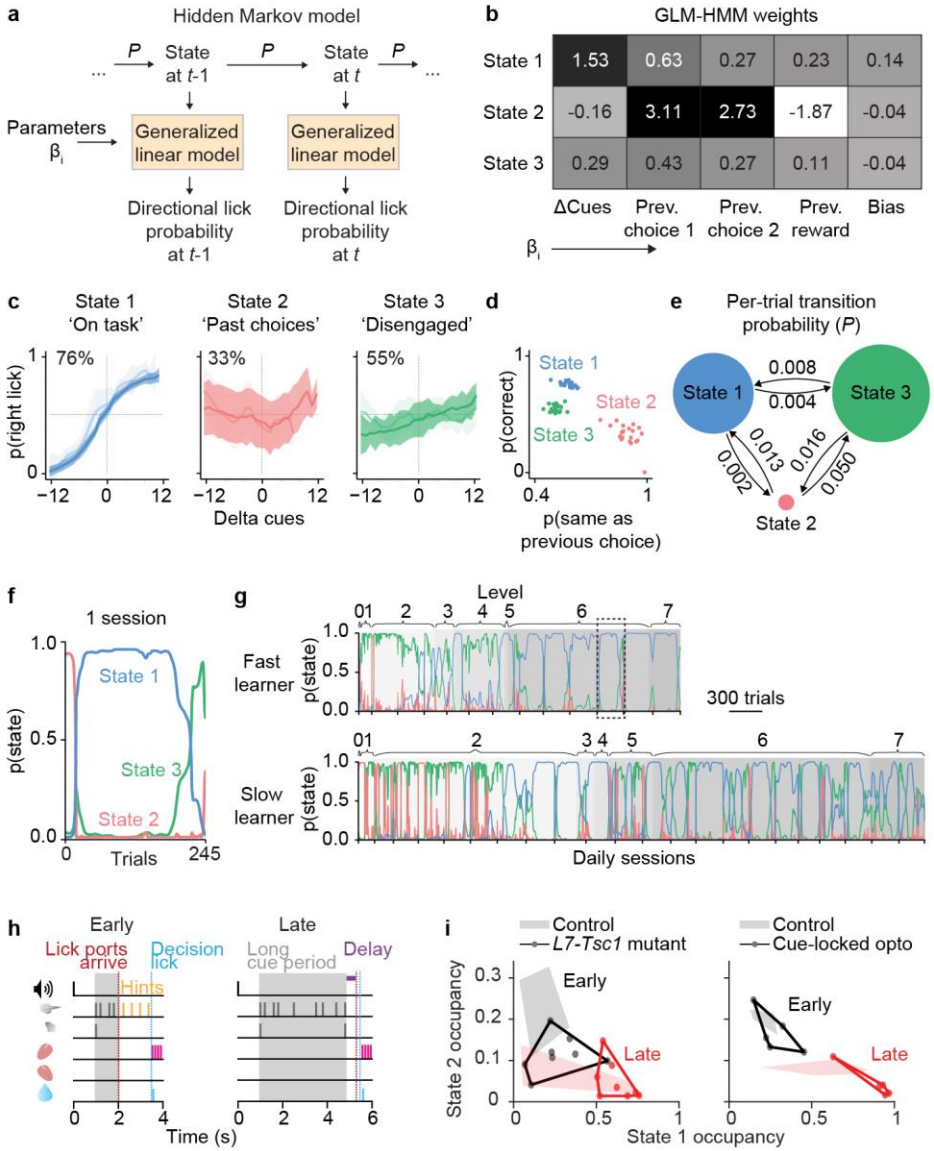

Fig. 4 | Latent behavioral-state analysis of task learning shows increased on-task focus in faster learners with cerebellar manipulations. a, Schematic illustrating the GLM-HMM. *P* is state transition probability. **b,** Inferred GLM-HMM weights from the training data set. **c,** Psychometric curves averaged across all mice. In the top left is the percentage correct over all trials in that state. Shaded areas represent one s.d. Lighter curves indicate early trials and darker curves indicate late trials (see panel **h**). **d,** Probability of a correct choice against the probability that the choice in the current trial was the same as the choice in the previous trial. Each data point represents the average across all trials for one mouse. **e,** Per-trial transition rate between the three states averaged over all mice. The size of the circles indicate state occupancy across all trials of the mice in the training data set. **f,** Posterior state probabilities for one example session. **g,** Posterior state probabilities for all trials in all sessions from a fast learner (top) and a slow learner (bottom). The dashed area in the top panel indicates the session in **f**. **h,** Two different stages of the evidence-

accumulation task. **i,** State 1 and state 2 occupancy during early and late stages for *L7-Tsc1* animals (left) and mice with cue-locked optogenetic activation of Purkinje cells in crus I (right). Each data point represents one mouse. Shaded areas indicate the area covered by control animals.

At the early stages of learning, animals mostly occupied state 2 or 3 until they made a transition to consistent state 1 occupancy (Fig. 4g,i). This shift in state occupancy occurred in all animals, and took more trials for slower learners (examples in Fig. 4g). Teaching the evidence-accumulation task to animals can be divided into two stages of task shaping: early, during which the animals still receive hint puffs to guide their choice, and late, during which animals need to accumulate the evidence in progressively more difficult trials (Fig. 4h). *L7-Tsc1* mutant mice already had higher state 1 occupancy than wild-type mice at the earliest stages of training, and this increased occupancy continued throughout the late stages (Fig. 4i, left and Extended Data Fig. 8a). The shape of the psychometric curves of *L7-Tsc1* mutant mice in each state was similar to their wild-type littermates (Extended Data Fig. 5).

Cerebellum-driven acceleration of learning might arise from enhancement of immediate cue experience, or alternately require longitudinal shaping across sessions. To distinguish these possibilities, we optogenetically reinforced each cue, but starting only after mice had passed out of the early stage of training. We found that mice showed an immediate tendency toward increased occupancy of on-task state 1 and reduced occupancy of prior-trial state 2 (Extended Data Fig. 8b). Specifically, 4 out of 5 optogenetically-reinforced mice spent more than 90% of the trials in state 1 and less than 5% of the trials in state 2 (Fig. 4i, right). This tendency continued through the rest of late training. In separate experiments, untreated animals which received stronger (20 psi) air puffs in late training also showed elevated current-trial-state occupancy throughout training (Extended Data Fig. 6c and Extended Data Fig. 8c).

When Purkinje cells in crus I are optogenetically stimulated in trained mice during the entire cue period and delay period including the first lick (Extended Data Fig. 7a), performance is impaired by forgetting immediately-past experience[9]. Even though such continuous stimulation increased overall simple-spike activity, it did not enhance simple-spike responses to individual sensory cues, and there was no change in complex spike firing in response to whisker puffs (Extended Data Fig. 7c,d) and no detectable effect on the learning rate (Extended Data Fig. 7b) or whisker puff responses in forebrain areas (Extended Data Fig. 7e,g,h). At levels with optogenetic stimulation, there was no change in state 1 occupancy, although there was a reduction in state 2 occupancy (Extended Data Fig. 6f and Extended Data 8d). In summary, under all conditions that accelerated learning, reduction in state 2 occupancy was visible at the earliest stages of perturbation (Extended Data Fig. 8).

Cerebellum, global coherence, and autism

Our experiments support the idea that cerebellar complex-spike output can accelerate learning through altered forebrain activity and increased on-task focus. Cerebellar activity is transmitted to neocortical structures via major paths through thalamus and other midbrain structures[15,28] that may convey these influences. Among the extensive neocortical targets of cerebellar projections is the parietal cortex, where, interestingly, silencing of activity was recently shown to improve performance in evidence accumulation by reducing reliance on past evidence[29]. Cerebellum and neocortex project to one another bidirectionally in a loopwise manner via thalamus, pons, and midbrain structures[30,31], including distributed influence of lobules over diverse associative and premotor regions[15]. Such connectivity provides a substrate for delayed activation

and spatially distributed responses. Indeed, in *L7-Tsc1* mutant mice, inhibition of the medial prefrontal cortex has previously been found to improve social deficits and repetitive behaviors[32].

In the central coherence account of autism spectrum disorder, the capacity to extract global form and meaning is displaced by superiority on local or detail-focused processing[1]. Our work in a mouse ASD model demonstrates one aspect of such processing, sensory hypersensitivity[2], and an association with accelerated capacity to learn a sensory-integration task. Our results also show one predicted feature of such increased sensitivity, hyperreactivity of local neocortical circuits[33]. The atypicalities of sensation and perception reported in ASD can be interpreted in terms of a broadening of Bayesian priors about the sensory world. "Hypo-priors" can account for a tendency among autistic persons "to perceive the world more accurately rather than [be] modulated by prior experience"[34]. In this way, autistic people see the world more accurately on an immediate basis, a trait that can both impair everyday life and lead to high performance in specific skill domains. The potential for variation in a brain trait to both disrupt features of everyday life and enhance specific skill domains recasts autism spectrum disorder not so much as a disorder but as a variation that, in particular niches, can be adaptive[1] (Extended Data Fig. 9).

Acknowledgements

We thank members of the Wang lab and the BRAIN CoGS consortium for discussion and advice, G. Joseph Broussard, Caroline Jung, Junuk Lee, Laura Lynch, Dafina Pacuku, and John Wuethrich for help with experiments, Jonathan Pillow for advice on latent-state analysis, Zahra Dhanerawala, Austin Hoag, and Sanjeev Janarthanan from the BRAIN CoGS Histology Core for brain clearing, imaging and probe localization, and Carlos Brody, Sabine Kastner, Manuel Schottdorf and Thomas Zhihao Luo for comments on the manuscript. The work was supported by National Institutes of Health grants R01 NS045193, R01 MH115750, and U19 NS104648 to SW, and European Union's Horizon 2020 research and innovation programme under the Marie Skłodowska-Curie grant agreement No 844318 to MO.

Author contributions

S.W. conceptualized the research. M.O., S.W., M.K. and B.D. designed the experiments. M.O., M.K. and T.C. performed the experiments. M.O. and Y.C. did data analysis and visualization. S.J.V. provided the code for the GLM-HMM analysis. M.O. and S.W. did funding acquisition, project administration, and supervision. S.W. and M.O. wrote the original draft, and M.O., Y.C., and B.D. reviewed and edited the paper.

Competing interests

Authors declare no competing interests.

Methods

Mice. Experimental procedures were approved by the Princeton University Institutional Animal Care and Use Committee (protocol 1943-19) and performed in accordance with the animal welfare guidelines of the National Institutes of Health and in line with the European Directive 2010/62/EU on the protection of animals used for experimental purposes.

Data came from 133 mice (males and females, 2 – 5 months of age at the start of experiments) of genotypes *C57BL/6J* (The Jackson Laboratory, Bar Harbor, ME, 40 animals), *Pcp2-Cre* for Purkinje-cell specificity and *Ai27D* for channelrhodopsin-2 (33 animals *Pcp2-Cre* x *Ai27D*, acquired from The Jackson Laboratory, stock #010536 (RRID:IMSR_JAX:010536) and #012567 (RRID:IMSR_JAX:012567), respectively) and $L7^{Cre}$;$Tsc1^{flox/flox}$ mice (60 animals). To create these Purkinje cell specific $L7^{Cre}$;$Tsc1^{flox/flox}$ mice, $Tsc1^{flox/flox}$ ($Tsc1^{tm1Djk}$/J, The Jackson Laboratory stock #005680) mutant mice were crossed into L7-Cre mice (B6.129-Tg(Pcp2-cre)2Mpin/J, The Jackson Laboratory, stock #004146). Experimenters were blinded to the genotypes of the mice for the duration of the behavioral experiments.

All mice were group-housed in reverse light cycle to promote maximal performance during behavioral testing, which took time during the day. For long-term behavioral experiments, mice were housed in darkness in an enrichment box containing bedding, houses, wheels (Igloo and Fast-Trac; K3250/K3251; Bio-Serv; Flemington, NJ, USA), climbing chains, and play tubes during all experimental days. At other times, mice were housed in cages in the animal facility, in groups of 2–4 mice per cage. During experiments in which water intake was restricted, mice received 1.0–1.5 mL of filtered water per day plus half of a mini yogurt drop (F7577; Bio-Serv;

Flemington, NJ, USA), and body weight (aimed at 85% of baseline body weight) and condition was monitored daily. Mice always had *ad libitum* access to food pellets.

Surgical procedures. For all surgeries, mice were anesthetized with isoflurane (5% for induction, 1.0 – 2.5% for maintenance), and were given buprenorphine (0.1 mg/kg body weight) and rimadyl (5 mg/kg body weight) after surgery and were given at least 5 days of recovery in their home cages before the start of experiments, except for acute *in vivo* electrophysiology experiments when the animals were allowed to recover for at least two hours between the craniotomy and the acute recordings.

For optogenetic experiments, a custom-machined titanium headplate[35] was cemented to the skull using dental cement (C and B Metabond, Parkell Inc). Two ~500 μm diameter craniotomies were drilled over the cerebellum, one over each hemisphere, directly posterior to the lamboid suture and ~3.6mm lateral to the midline in either direction. Ferrule implants were constructed with 400-μm-diameter optical fiber (Thorlabs FT400EMT) glued to 1.25-mm OD stainless steel ferrules (Precision Fiber Products MM-FER2007-304-4500) using epoxy (Precision Fiber Products PFP 353ND). Ferrules were positioned over each craniotomy with the fiber tip at the surface of the dura mater, and Vetbond (3 M) was applied surrounding the exposed fiber. Dental cement was then applied to secure the ferrule to the skull. Implants were cleaned before each behavior session using a fiber optic cleaning kit (Thorlabs CKF).

For *in vivo* electrophysiology, a headplate was implanted as described above, and a 2 mm craniotomy was drilled over the area of interest and the dura removed. For recordings from neocortex, the following stereotaxic coordinates were used: anterior cingulate cortex: ML 0 – 0.5 mm, AP 0.5 – 1.5 mm, DV 0.7 – 1.0 mm, anterolateral motor cortex: ML 1.5 mm, AP 2.5 mm,

DV 0.7 – 1.0 mm, and barrel field of the primary somatosensory cortex: ML 2.5 – 3.5 mm, AP -0.8 – -1.8 mm, DV 0.6 – 1.5 mm. Two stainless steel screws for ground and reference wires (000–120 1/16 SL bind machine screws, Antrin miniature specialties, Inc) were inserted in the skull above the forebrain as far away from the craniotomy as possible. For cerebellar recordings, a small hole was drilled for a reference electrode in the interparietal bone at the midline. Craniotomies (0.5 mm by 1 – 1.5 mm) were made next to the intersection of interparietal and occipital bones and over the left and right lobule V and simplex for extracellular single-unit recordings. Craniotomies were covered with Kwik-Cast silicone adhesive (World Precision Instruments) until the time of the recording.

Behavior experiments. Mice were trained to perform an evidence-accumulation decision-making task as described previously[5,9]. The behavioral apparatuses were controlled by custom-written Python software as published previously[5] (https://github.com/wanglabprinceton/accumulating_puffs). Animals were trained for 1.5 – 9 weeks, 7 days/week. Briefly, head-fixed mice were seated in a tube for daily one-hour behavioral sessions consisting of 200 – 300 trials. In each trial, independent streams of randomly timed 40-ms air puffs of 10 psi (unless otherwise indicated) with a minimum 200 ms interpuff interval were delivered to the left and right sides over the course of a 1.0 – 3.8-second cue period. After a delay period of 200 – 800 ms, lick ports were advanced into the reach of the animal, and animals received a 4 µl water reward when they licked to the side with the greater number of puffs. The animal's decision was interpreted as the side licked first, regardless of subsequent licks. Anti-biasing procedures[5] result in chance levels being < 50%. To increase motivation, restriction of

water intake started at least 5 days before the start of training and continued throughout the whole training period.

Animals went through different levels of training (levels 0 – 6) to reach the final version of the task (level 7). Mice automatically proceeded to the next level once they reached pre-defined performance criteria (see Extended Data Table 1 for details of each level as well as the performance criteria). The time it took an animal to learn the task was defined as the total number of trials to reach level 7. For experiments with air puffs at 20 psi, stronger air puffs were delivered at every trial starting at level 3.

Light for optogenetic stimulation during the evidence-accumulation task was delivered as described previously[9]. Cue-locked optogenetic activation occurred unilaterally, at the same side and time at an air puff, for a duration of 40 ms (generated by Master-8, A.M.P.I.). Continuous optogenetic activation occurred bilaterally with 5-ms pulses at 50 Hz throughout the entire cue period, delay period, and ended upon first lick contact. When optogenetic activation was used to manipulate the learning rate, the optogenetic activation only started from level 3, and at every trial from then on. When optogenetic activation was used to manipulate performance in trained mice (Fig. 3f), light was on in 20% of trials. In this case, analysis compares light-off and light-on trials only from behavioral sessions in which light was delivered.

For the delay tactile startle conditioning (DTSC) task[21], mice learned to elicit a startle (backward) movement in response to an initially neutral conditioned stimulus (CS; 250 ms; 5mm 395 – 400nm UV Ultraviolet LED, EDGELEC) that was paired with a startle-eliciting unconditioned stimulus (US, 20 ms tactile stimulus on the nose by taping foam that was attached to the stepper motor shaft (High Torque Nema 17 Bipolar Stepper Motor 92oz.in/65Ncm 2.1A Extruder Motor, Stepper Online); CS-US inter-stimulus interval, 200 ms).

For sensory sensitivity tests, naive animals were headfixed in a similar setup to the evidence-accumulation setup and received either whisker puffs or auditory cues. Animals were not trained nor expected to do anything in response to the sensory cues, and did not receive any rewards throughout the session. Animals received cues in sequences of in total 24 cues starting and ending with three cues with 200 ms inter-cue interval, and in between those, cues at random intervals (ranging from 0.8 to 3 s). Animals first received a sequence with cue durations of 8 ms, followed by sequences with longer cue durations (15, 30, and 45 ms for whisker puffs, and 15, 30, 45, 90, 180, 320, and 640 ms for auditory cues). Animals either received bilateral air puffs to the whiskers at 20 – 25 psi, or auditory cues at 12 kHz. During sensitivity tests with whisker puffs, white noise was on in the background throughout the experiment. To determine eye blink responses, movies of the right side of their face and body were acquired using two USB cameras (Playstation Eye), modified by removal of infrared filters and encasings. Images were acquired at 30 Hz with 320 × 240 pixel resolution. Illumination was provided by an infrared LED array (Yr.seasons 48-LED Illuminator Light CCTV 850 nm IR Infrared Night Vision). Air puffs were produced by activation of solenoids (NResearch, standard two-way normally closed isolation valve, 161T011) with input from an air source (ControlAir Type 850 Miniature Air Pressure Regulator). Air was delivered via two tubes custom-machined with uniform openings, and positioned parallel to one another, parallel to the anteroposterior axis of the animal, 10 mm apart mediolaterally and ~1 mm anterior to the nose of the animal. Auditory cues were delivered to the apparatus by a speaker (Sony Tweeter XS-H20S) mounted below the apparatus. Analysis of eye blinks was performed using FaceMap (https://github.com/MouseLand/facemap)[36] with manual curation and further analysis in Python.

***In vivo* electrophysiology.** For acute recordings from awake behaving mice, animals were head-fixed over a freely rotating cylindrical treadmill and the craniotomy site was opened by removing the Kwik-Cast plug and then filled with saline. Recordings were performed using either silicon probes for neocortex or glass electrodes for cerebellum, as described below. Air puffs to the whiskers were delivered by a pressure injector system (Toohey Spritzer, Toohey, Fairfield, NJ, USA) which received signals from a signal generator (Master-8; AMPI) with an intensity of 20 psi and a frequency of 1 Hz, except for experiments with continuous optogenetic activation throughout the entire cue and delay period, when air puffs were delivered with a frequency of 0.2 Hz. Mice received unilateral air puffs ipsilaterally to the recording site for Purkinje cells, anterior cingulate cortex, and anterolateral motor cortex, and contralaterally to the recording site for cerebellar nuclei and the barrel field of the somatosensory cortex. For recordings with optogenetic stimulation, light onset started at the same time as the air puff for the duration of the air puff (40ms) unless indicated otherwise. In a subset of experiments (Extended Data Fig. 4d) light started at the same time as the air puff but remained on for longer (250 ms).

For neocortical recordings, a 64-channel silicon probe (Neuronexus, A4x16-5mm-50-200-177 or A2x32-Poly5-10mm-20s-200-100) covered in Vybrant™ CM-DiI Cell-Labeling Solution (V22888; Invitrogen) was slowly placed above the craniotomy and lowered into the brain using a motorized micromanipulator (MP-225; Sutter Instrument Co.). The silicon probes were connected to two amplifier boards (RHD2132, Intan Technologies) using a dual headstage adapter (RHD2000, Intan Technologies). Recordings were made using an Open Ephys acquisition board at a sampling rate of 30 kHz. High-pass filtering of the raw data at 300 Hz, common median referencing, and automatic spike sorting was achieved using Kilosort 2 (https://github.com/cortex-lab/Kilosort)[37]. Spikes were further manually curated using the Phy

GUI (https://github.com/kwikteam/phy). Neocortical recording locations were verified post mortem by identifying the CM-DiI fluorescence in cleared brains (see histology section below).

Single-unit recordings of Purkinje neurons and cerebellar nuclei neurons were performed using borosilicate glass electrodes (1B100F-4, World Precision Instruments) with 1 – 2-µm tips, short for Purkinje cells or very long gradual tapers for cerebellar nuclei cells, and 3 to 12 MΩ impedance, fabricated on a pipette puller (P-2000, Sutter Instruments Co.) and filled with sterile saline. The electrode was lowered into the cerebellum using an electrode holder that was positioned at a 40 or 90° angle to the craniotomy and controlled by a motorized micromanipulator (MP-225; Sutter Instrument Co.). The obtained electrical signals were amplified with a CV-7B headstage and Multiclamp 700B amplifier, digitized at 10 kHz with a Digidata 1440A and acquired in pClamp (Axon Instruments, Molecular Devices) in parallel with transistor-transistor logic (TTL) pulses from a signal generator (Master-8; AMPI) and with signal from pressure injector system (Toohey Spritzer, Toohey, Fairfield, NJ, USA). Purkinje neurons were identified by the presence of complex spikes followed by a characteristic pause in simple spikes. The cerebellar nuclei contain a high density of neurons that are deeper than and well separated from cerebellar cortical layers, and show clear single unit spike activity. Spike detection was performed using custom code written in MATLAB 2019a.

Histology. Animals were anesthetized with an overdose of ketamine (400 mg/kg)/xylazine (50 mg/kg) (i.p.) and transcardially perfused using a peristaltic pump with phosphate buffered saline (PBS) with 10 mg/ml heparin (Sigma H3149-100KU), followed by chilled 10% formalin (Fisher Scientific). Brains were extracted from the skull after perfusion, postfixed overnight at 4°C, washed and stored in PBS at room temperature. To visualize the probe locations using the CM-

DiI track, brains were cleared and imaged by the BRAIN CoGS histology core facility. All brains underwent the same abbreviated iDISCO+ clearing protocol as previously described[15]. In short, after an overnight fix in 4% PFA, brains were rinsed in PBS at room temperature for four 30 minute sessions. Immediately brains were dehydrated 1 hour at each ascending concentration of methanol (20, 40, 60, 80, 100, 100%) and placed overnight in methanol at room temperature. The next day, they were being placed in 66% dichloromethane (DCM)/33% methanol for 3 hours at room temperature. Brains were cleared with 100% DCM for two 15 minute steps then placed in 100% benzyl ether (DBE). Brains were kept in fresh DBE prior to imaging and after for long-term storage. Tissue was imaged using a light-sheet microscope (Ultramicroscope II, LaVision Biotec., Bielefeld, Germany).

For quantification of Purkinje cells, Purkinje cells were stained with calbindin. Animals were transcardially perfused as described above, and after postfixation were stored in PBS at 4°C until sectioning. Whole brain sagittal sections were cut at 90 μm and collected in 0.1 M PBS. Sections were processed for immunohistology by washing with PBS and incubating for 1 hour at room temperature in a blocking buffer (10% normal goat serum, 0.5% Triton in PBS) prior to a 2-day incubation at 4°C in PBS buffer containing 2% NGS, 0.4% Triton and the rabbit anti-calbindin-D-28K primary antibody (C7354; Sigma-Aldrich St. Louis, MO, USA; 1:1000). Sections were subsequently washed in PBS, incubated for 2 hours at room temperature in the PBS buffer with goat anti-rabbit Alexa Fluor 488-conjugated secondary antibody (A-11008; Thermo Fisher Scientific, MA, USA, Invitrogen; 1:400), mounted on glass slides and covered with Vectashield. Images were acquired on the epifluorescent microscope Hamamatsu Nanozoomer. Using NDP.view2 Plus software, individual lobules were identified and Purkinje cells were assigned to lobules for counting.

Corticosterone measurements. Animals were food deprived for 12 – 24 hours before blood collection. Immediately after receiving air puffs to whiskers at 20 – 25 psi in a headfixed setup for 10 – 20 minutes, ~50 µl of blood was collected from the tail vein using a capillary tube, and then immediately disposed of in a heparin-coated 1.5 ml eppendorf tube. Samples were stored on wet ice for maximum 4 hours, after they were centrifuged for 10 minutes at 4 ºC at 3000 rpm. Of each sample 2 – 10 µl of plasma was collected, placed in new non-coated 1.5 ml eppendorf tubes and stored at -80 ºC. For each animal, two duplicate samples of 1 µl each were used to determine plasma corticosterone levels using the Corticosterone ELISA Kit (K014; Arbor Assays, Ann Arbor, MI, USA) according to the manufacturer's protocol. Plate reading was done using an Infinite 200Pro (Tecan Life Sciences, Morrisville, NC, USA) with i-control software. Results from both duplicates were averaged to get one final corticosterone measurement per animal.

Generalized linear model - hidden Markov model. The generalized linear model - hidden Markov model (GLM-HMM) combines a set of Bernoulli GLMs with a hidden Markov model[6–8]. For each trial, the animal is modeled to have a latent state that governs its strategy to process information in order to make the binary choice of which side to lick. Each state corresponds to a specific GLM with a unique weight vector of input variables. Between trials, the transition matrix of HMM defines the probability to change from one state to another. The output of GLM-HMM in each trial is calculated as the probability of a Bernoulli response (i.e. the probability of a rightward lick) based on both the latent state of current trial and the input variables. Delta cues (Δ cues) is the number of air puffs on the right side minus the number of air puffs on the left side. Guide air puffs ('hints') are included. Previous choice 1 is the animal's choice on the previous trial. Previous choice 2 is the animal's choice of the trial prior to the previous trial.

Previous reward is the side of the reward on the previous trial. Bias is an offset constant in each state that represents the tendency to lick rightward independent of other input variables. The trials used to calculate the psychometric curve of a latent state are selected to have a posterior probability for that state larger than 0.8. The state occupancy of a certain state is calculated as the fraction of trials whose posterior state probabilities are greatest for that state. The model is trained with the data of 22 wild-type mice on the air puff evidence accumulation task and fitted using expectation–maximization algorithm with code adapted from https://github.com/Brody-Lab/venditto_glm-hmm.

Statistical analysis and presentation. Statistical tests used are indicated throughout the text. All further analysis was done with custom-written code in Python 3 using Spyder (https://www.spyder-ide.org/), and R (https://www.r-project.org/) using RStudio (https://www.rstudio.com/). For every figure, * = $P \leq 0.05$, ** = $P \leq 0.01$, *** = $P \leq 0.001$. Box and whiskers show median/interquartile range, and 1.5x the interquartile range. The left panel of Fig. 1a was created with BioRender.

Code and data availability. Code used for data acquisition is available at https://github.com/wanglabprinceton/accumulating_puffs. All data that support the findings of this study are available from the corresponding authors on reasonable request.

References

1. Happé, F. & Frith, U. The weak coherence account: detail-focused cognitive style in autism spectrum disorders. *J. Autism Dev. Disord.* **36**, 5–25 (2006).
2. Mottron, L., Dawson, M., Soulières, I., Hubert, B. & Burack, J. Enhanced perceptual functioning in autism: an update, and eight principles of autistic perception. *J. Autism Dev. Disord.* **36**, 27–43 (2006).
3. Limperopoulos, C. *et al.* Does cerebellar injury in premature infants contribute to the high prevalence of long-term cognitive, learning, and behavioral disability in survivors? *Pediatrics* **120**, 584–593 (2007).
4. Wang, S. S.-H., Kloth, A. D. & Badura, A. The cerebellum, sensitive periods, and autism. *Neuron* **83**, 518–532 (2014).
5. Deverett, B., Koay, S. A., Oostland, M. & Wang, S. S.-H. Cerebellar involvement in an evidence-accumulation decision-making task. *eLife* **7**, e36781 (2018).
6. Ashwood, Z. C. *et al. Mice alternate between discrete strategies during perceptual decision-making*. 2020.10.19.346353 https://www.biorxiv.org/content/10.1101/2020.10.19.346353v3 (2021) doi:10.1101/2020.10.19.346353.
7. Calhoun, A. J., Pillow, J. W. & Murthy, M. Unsupervised identification of the internal states that shape natural behavior. *Nat. Neurosci.* **22**, 2040–2049 (2019).
8. Bolkan, S. S. *et al. Strong and opponent contributions of dorsomedial striatal pathways to behavior depends on cognitive demands and task strategy*. 2021.07.23.453573 https://www.biorxiv.org/content/10.1101/2021.07.23.453573v1 (2021) doi:10.1101/2021.07.23.453573.
9. Deverett, B., Kislin, M., Tank, D. W. & Wang, S. S.-H. Cerebellar disruption impairs

working memory during evidence accumulation. *Nat. Commun.* **10**, 3128 (2019).

10. Heijden, M. E. van der, Gill, J. S. & Sillitoe, R. V. Abnormal cerebellar development in autism spectrum disorders. *Dev. Neurosci.* **43**, 181–190 (2021).
11. Carta, I., Chen, C. H., Schott, A. L., Dorizan, S. & Khodakhah, K. Cerebellar modulation of the reward circuitry and social behavior. *Science* **363**, (2019).
12. Hatten, M. E. Adding cognitive connections to the cerebellum. *Science* **370**, 1411–1412 (2020).
13. Küper, M. & Timmann, D. Cerebellar mutism. *Brain Lang.* **127**, 327–333 (2013).
14. Garfinkle, J. *et al.* Location and size of preterm cerebellar hemorrhage and childhood development. *Ann. Neurol.* **88**, 1095–1108 (2020).
15. Pisano, T. J. *et al.* Homologous organization of cerebellar pathways to sensory, motor, and associative forebrain. *Cell Rep.* **36**, (2021).
16. Badura, A. *et al.* Normal cognitive and social development require posterior cerebellar activity. *eLife* **7**, e36401 (2018).
17. Tsai, P. T. *et al.* Autistic-like behaviour and cerebellar dysfunction in Purkinje cell Tsc1 mutant mice. *Nature* **488**, 647–651 (2012).
18. Kloth, A. D. *et al.* Cerebellar associative sensory learning defects in five mouse autism models. *eLife* **4**, e06085 (2015).
19. Klibaite, U. *et al. Deep behavioral phenotyping of mouse autism models using open-field behavior*. 2021.02.16.431500 https://www.biorxiv.org/content/10.1101/2021.02.16.431500v1 (2021) doi:10.1101/2021.02.16.431500.
20. Pinto, L. *et al.* An accumulation-of-evidence task using visual pulses for mice navigating in

560 virtual reality. *Front. Behav. Neurosci.* **12**, 36 (2018).

561 21. Yamada, T. *et al.* Sensory experience remodels genome architecture in neural circuit to drive
562 motor learning. *Nature* **569**, 708–713 (2019).

563 22. Kim, O. A., Ohmae, S. & Medina, J. F. A cerebello-olivary signal for negative prediction
564 error is sufficient to cause extinction of associative motor learning. *Nat. Neurosci.* **23**, 1550–
565 1554 (2020).

566 23. Llinas, R. The olivo-cerebellar system: a key to understanding the functional significance of
567 intrinsic oscillatory brain properties. *Front. Neural Circuits* **7**, 96 (2014).

568 24. Kennerley, S. W., Walton, M. E., Behrens, T. E. J., Buckley, M. J. & Rushworth, M. F. S.
569 Optimal decision making and the anterior cingulate cortex. *Nat. Neurosci.* **9**, 940–947
570 (2006).

571 25. Chabrol, F. P., Blot, A. & Mrsic-Flogel, T. D. Cerebellar contribution to preparatory activity
572 in motor neocortex. *Neuron* **103**, 506-519.e4 (2019).

573 26. Gao, Z. *et al.* A cortico-cerebellar loop for motor planning. *Nature* **563**, 113–116 (2018).

574 27. Bengtsson, F. & Hesslow, G. Cerebellar control of the inferior olive. *The Cerebellum* **5**, 7–14
575 (2006).

576 28. Fujita, H., Kodama, T. & du Lac, S. Modular output circuits of the fastigial nucleus for
577 diverse motor and nonmotor functions of the cerebellar vermis. *eLife* **9**, e58613 (2020).

578 29. Akrami, A., Kopec, C. D., Diamond, M. E. & Brody, C. D. Posterior parietal cortex
579 represents sensory history and mediates its effects on behaviour. *Nature* **554**, 368–372
580 (2018).

581 30. Strick, P. L., Dum, R. P. & Fiez, J. A. Cerebellum and nonmotor function. *Annu. Rev.*
582 *Neurosci.* **32**, 413–434 (2009).

583 31. Wagner, M. J. & Luo, L. Neocortex-cerebellum circuits for cognitive processing. *Trends*
584 *Neurosci.* **43**, 42–54 (2020).
585 32. Kelly, E. *et al.* Regulation of autism-relevant behaviors by cerebellar–prefrontal cortical
586 circuits. *Nat. Neurosci.* **23**, 1102–1110 (2020).
587 33. Markram, K. & Markram, H. The Intense World Theory – A Unifying Theory of the
588 Neurobiology of Autism. *Front. Hum. Neurosci.* **4**, (2010).
589 34. Pellicano, E. & Burr, D. When the world becomes 'too real': a Bayesian explanation of
590 autistic perception. *Trends Cogn. Sci.* **16**, 504–510 (2012).
591 35. Dombeck, D. A., Khabbaz, A. N., Collman, F., Adelman, T. L. & Tank, D. W. Imaging large
592 scale neural activity with cellular resolution in awake mobile mice. *Neuron* **56**, 43–57
593 (2007).
594 36. Stringer, C. *et al.* Spontaneous behaviors drive multidimensional, brain-wide activity.
595 *Science* **364**, 255 (2019).
596 37. Pachitariu, M., Steinmetz, N., Kadir, S., Carandini, M. & Harris, K. D. *Kilosort: realtime*
597 *spike-sorting for extracellular electrophysiology with hundreds of channels*. 061481
598 https://www.biorxiv.org/content/10.1101/061481v1 (2016) doi:10.1101/061481.

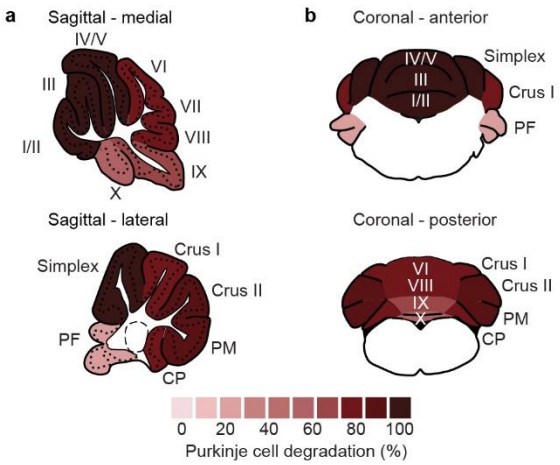

Extended Data Fig. 1 | Purkinje cell degeneration in *L7-Tsc1* mutant mice. a-b, Schematic of a sagittal (**a**) and coronal (**b**) view of the cerebellum with quantification of Purkinje cell loss averaged over 4 *L7-Tsc1* mutant mice at 5 – 6 months old for each cerebellar lobule, normalized to 3 wild-type littermates. C.M., copula pyramidis; P.F., flocculus & paraflocculus; P.M., paramedian lobule.

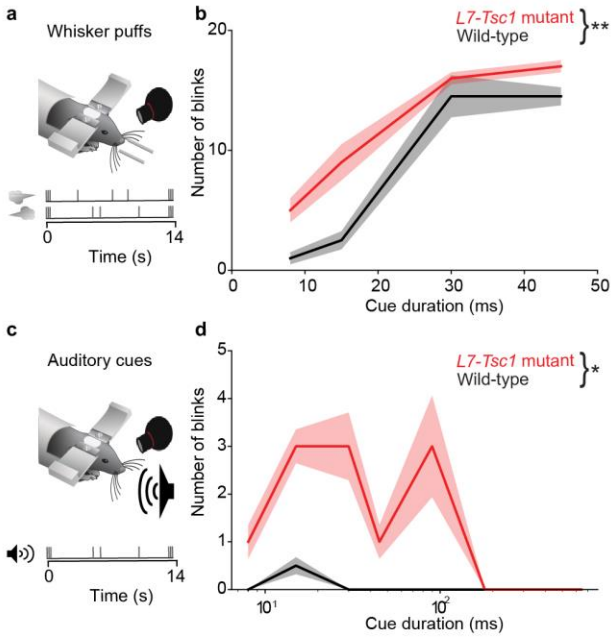

Extended Data Fig. 2 | Increased sensory sensitivity in *L7-Tsc1* mice. a, Schematic of sensory sensitivity test with bilateral and unilateral whisker puffs. **b,** Median number of eye blinks in response to whisker puffs of different durations for *L7-Tsc1* mutant mice (n = 16) and wild-type littermates (n = 7). A two-way ANOVA indicates an effect of genotype (F = 7.44, P = 0.008), as well as whisker puff duration (F = 32.795, P = 3.9×10^{-14}), but no interaction effect (F = 0.985, P = 0.4). **c,** Schematic of sensory sensitivity tests with auditory cues. **d,** Same as **b**, but for auditory cues. A two-way ANOVA indicates an effect of genotype (F = 5.06, P = 0.026), but not of audio cue duration (F = 1.697, P = 0.11) or an interaction effect (F = 0.347, P = 0.93). Shaded areas indicate the estimated s.e.m. using median absolute deviation.

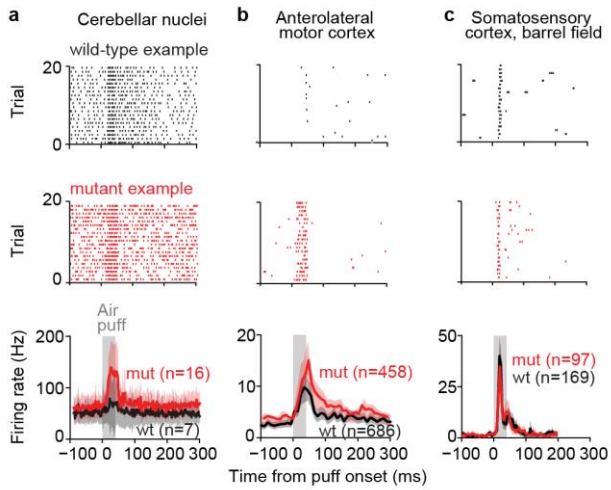

615

616 **Extended Data Fig. 3 | Increased responses to whisker puffs in *L7-Tsc1* mice in cerebellar**
617 **nuclei and anterolateral motor cortex, but not somatosensory cortex. a-c,** Example raster
618 plots of cerebellar nuclei cells (**a**), anterolateral motor cortex (**b**), and the barrel field of the
619 primary somatosensory cortex (**c**) during 20 trials from *L7-Tsc1* mutants (middle) or their wild-
620 type littermates (top), and average firing rates (bottom) in response to an air puff to the whiskers
621 (data from the same 4 *L7-Tsc1* mutants and 5 wild-type mice as in Fig. 2). Shaded areas
622 represent 95% confidence intervals.

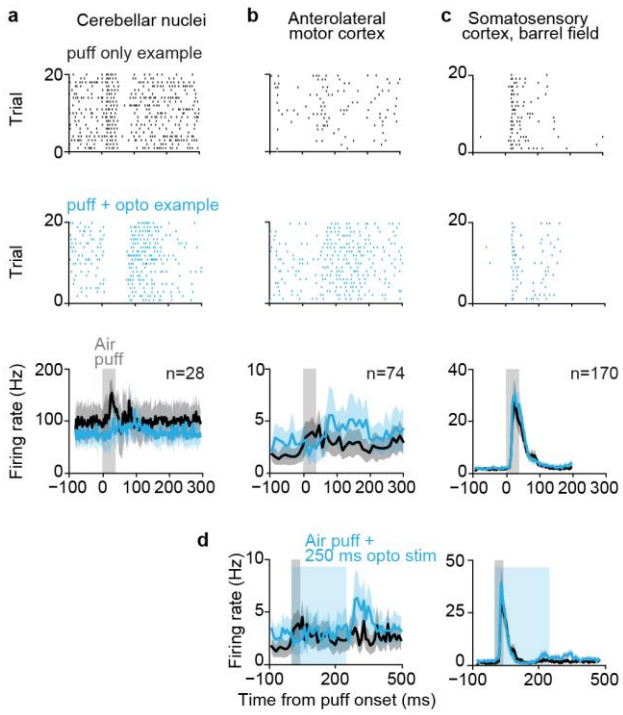

Extended Data Fig. 4 | Altered responses to whisker puff and cue-locked optogenetic stimulation of Purkinje cells in crus I in cerebellar nuclei and anterolateral motor cortex, but not somatosensory cortex. a-c, Example raster plots of cerebellar nuclei cells (**a**), anterolateral motor cortex (**b**), and the barrel field of the primary somatosensory cortex (**c**) during 20 trials with only a whisker puff (top) or with a whisker puff paired with optogenetic stimulation (middle), and average firing rates (bottom) in response to an air puff to the whiskers with or without paired optogenetic stimulation of Purkinje cells. **d,** Same as the bottom plots in **b** and **c**, but now with a longer duration (250 ms instead of 40 ms) of the optogenetic stimulation. Shaded areas represent 95% confidence intervals.

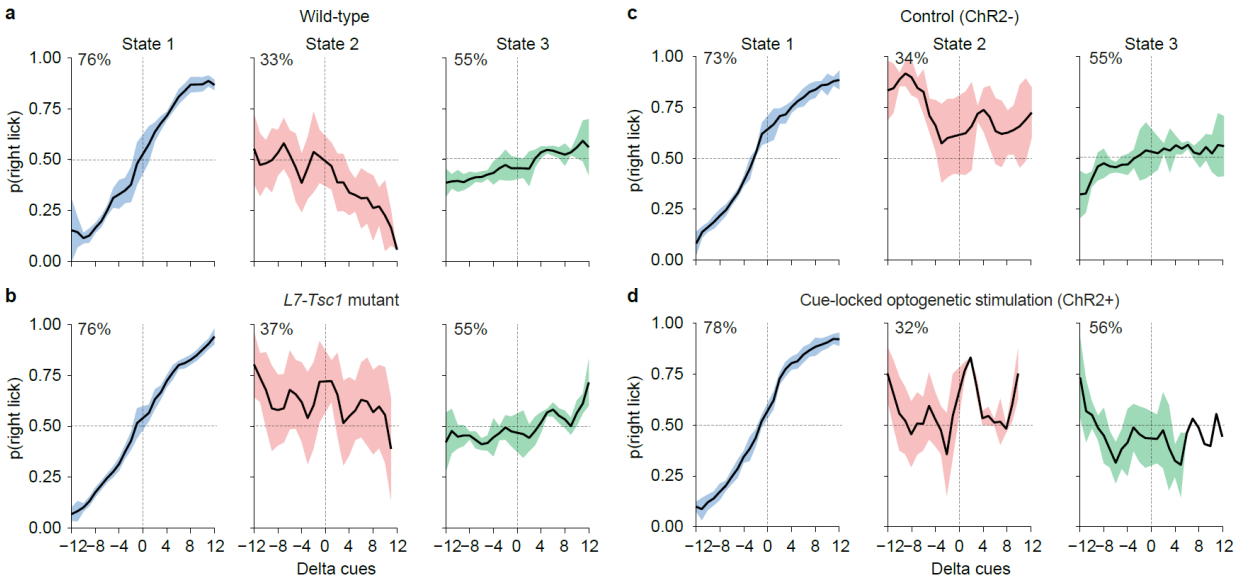

Extended Data Fig. 5 | Psychometric curves in the three states remain the same for *L7-Tsc1* mice and for mice receiving cue-locked optogenetic stimulation. a-d, Psychometric curves for the three states, averaged across all wild-type mice (**a**), *L7-Tsc1* mutant mice (**b**), ChR- mice (**c**) and ChR+ mice receiving cue-locked optogenetic stimulation of Purkinje cells in crus I (**d**). In the top left of each plot is the percentage correct over all trials in that state. Missing data points or data points without error bars indicate none or one animal at that data point due to low state occupancy. Shaded areas represent 1 s.d.

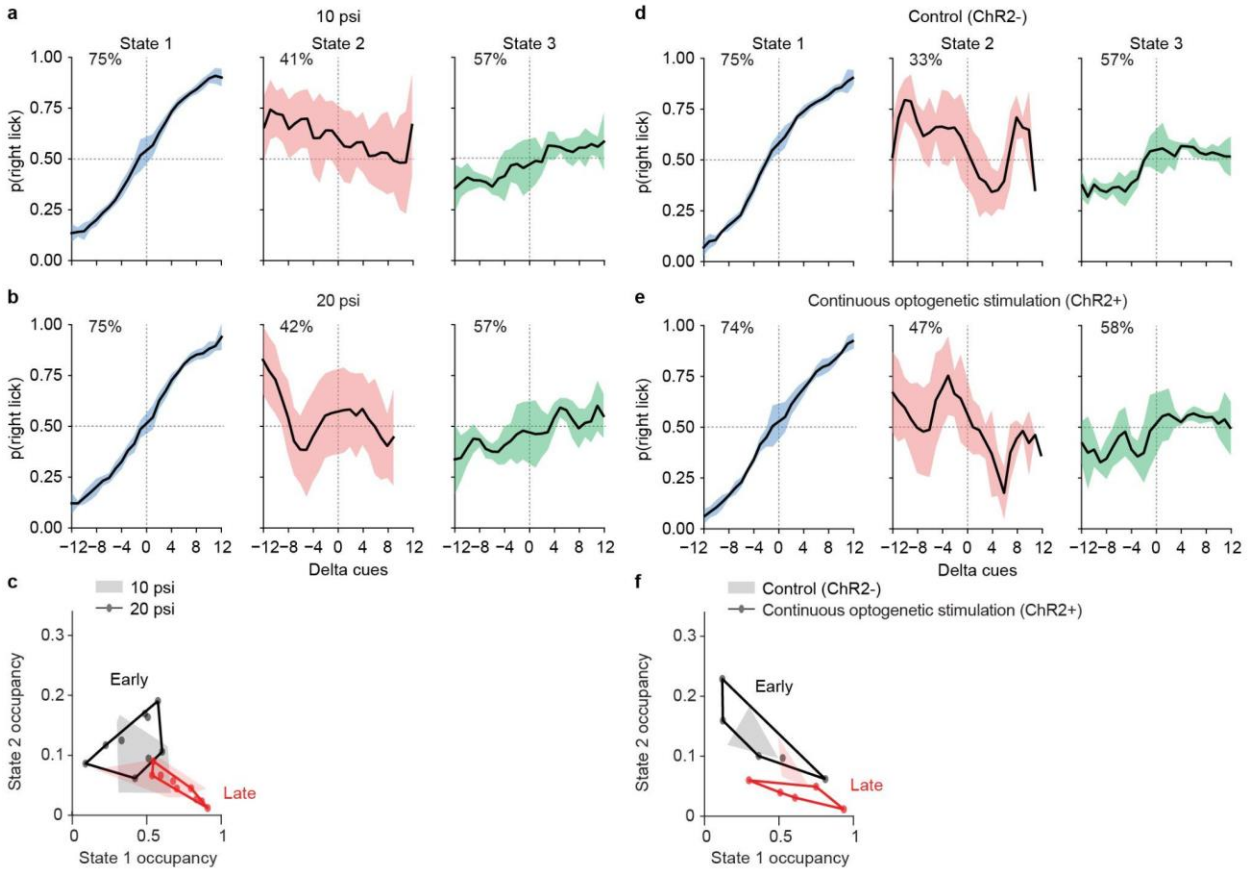

Extended Data Fig. 6 | Performance and state occupancy for animals receiving stronger whisker puffs or optogenetic stimulation of Purkinje cells in crus I throughout the entire cue period and delay period. a-d, Psychometric curves for the three states, averaged across all mice receiving air puffs to the whiskers of regular intensity (10 psi, **a**) or higher intensity (20 psi, **b**) or the normal task version for mice not expressing opsin (ChR2-) (**c**) or for mice expressing opsin (ChR2+) and receiving continuous optogenetic stimulation to Purkinje cells in crus I during the cue period, delay period, and first lick (**d**). In the top left of each plot is the percentage correct over all trials in that state. Shaded areas represent one standard deviation. **e-f,** State occupancy for mice receiving stronger whisker puffs (**e**), or optogenetic stimulation (**f**). Note that the manipulations did only occur in the late levels of the task. Shaded areas indicate the area covered by control animals.

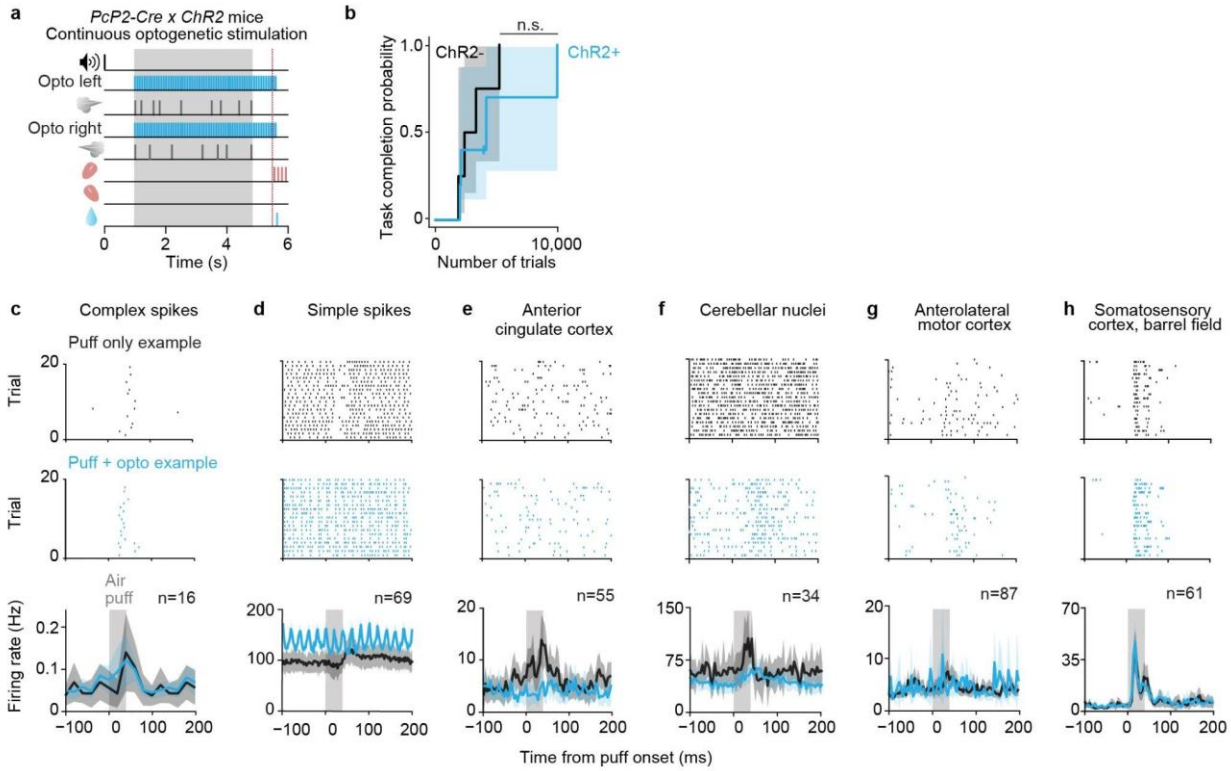

Extended Data Fig. 7 | No effect of continuous optogenetic activation of Purkinje cells in crus I on learning of the evidence-accumulation task. a, Schematic of the evidence-accumulation task with continuous bilateral optogenetic activation of crus I. **b,** Kaplan-Meier estimator of task completion probability for *PcP2-Cre* × *ChR2* mice with continuous bilateral optogenetic activation of crus I throughout the evidence-accumulation task (n = 5, median 4210 trials) compared to wild-type littermates (n = 4, median 2534 trials, $\chi^2(1) = 0.31$, $P = 0.33$, log-rank test). **c-h,** Example raster plots of Purkinje cell complex spikes (**c**), Purkinje cell simple spikes (**d**) anterior cingulate cortex (**e**), cerebellar nuclei cells (**f**), anterolateral motor cortex (**g**), and the barrel field of the primary somatosensory cortex (**h**) during 20 trials with only a whisker puff (top) or with a whisker puff paired with discounting optogenetic stimulation (middle), and average firing rates in response to an air puff to the whiskers with or without paired optogenetic stimulation of Purkinje cells. Shaded areas represent 95% confidence intervals.

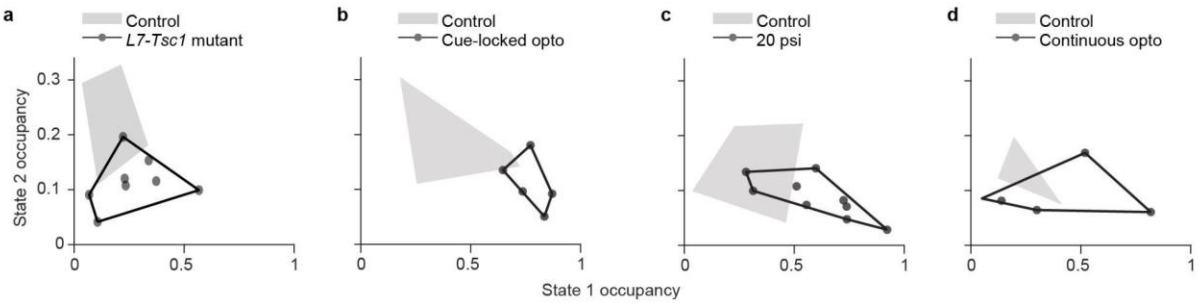

Extended Data Fig. 8 | Altered state occupancy occurs already at the earliest levels of manipulation. **a,** State occupancy at levels 0, 1, and 2 for *L7-Tsc1* mutant mice. **b,** State occupancy at levels 3 and 4 for animals receiving cue-locked optogenetic stimulation of crus I. **c,** State occupancy at levels 3 and 4 for animals receiving stronger air puffs (20 psi) to the whiskers. **d,** State occupancy at levels 3 and 4 for animals receiving bilateral optogenetic stimulation of crus I during the entire cue period, delay period, and first lick. Shaded areas indicate the area covered by control animals.

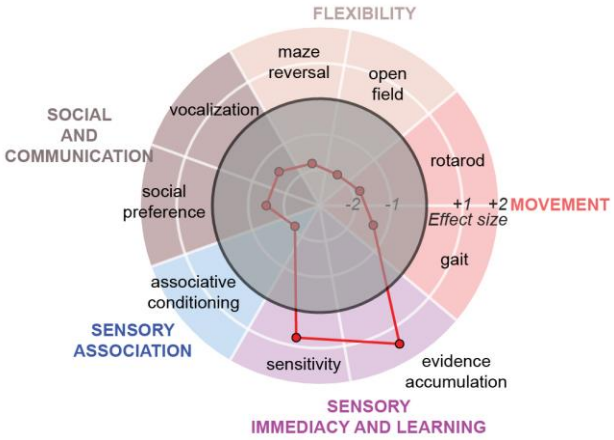

675

676 **Extended Data Fig. 9 | *L7-Tsc1* mutant mice have an island of enhanced sensory sensitivity**
677 **and learning combined with impaired association learning, social behaviors, flexibility, and**
678 **movement.** Each dot represents an estimated effect size (Cohen's *d*) for the behavior of *L7-Tsc1*
679 mutant mice compared to their wild-type littermates. The thick circle indicates typical behavior
680 (effect size 0). Based on data presented in this paper and from [17–19].

Extended Data Table 1 | Mice progress through eight different levels during learning of the evidence-accumulation decision-making task.

Level	0	1	2	3	4	5	6	7
Audio cue, 1s before cue period onset	Yes	Yes	Yes	Yes	Yes	Yes	Yes	Yes
Bilateral puffs at start	Yes	Yes	Yes	Yes	Yes	Yes	Yes	Yes
Cue period duration (s)	1	1	1	2.0, 2.8, or 3.8	3.8, or 1.5	3.8, or 1.5	3.8, or 1.5	3.8, or 1.5
Distractor puffs	No	No	No	No	No	No	Yes, 1:9	Yes, 1:4
Bilateral puffs at end	No	No	Yes	Yes	Yes	Yes	Yes	Yes
Delay (ms)	200	200	200	200	500	800	800	800
Guide puffs (2.5 Hz) until animal licks	No	Yes	Yes	No	No	No	No	No
Need to lick on correct side for reward	No	Yes	Yes	Yes	Yes	Yes	Yes	Yes
Does first lick need to be correct	No	No	Yes	Yes	Yes	Yes	Yes	Yes
Error trials punished	No	No	Yes	Yes	Yes	Yes	Yes	Yes
Requirements to proceed to next level	15 consecuti-ve rewards	at least 100 trials & 55% correct in window of 40 trials	at least 200 trials & 80% correct in window of 50 trials	at least 100 trials & 75% correct in window of 40 trials	at least 100 trials & 80% correct in window of 40 trials	at least 25 trials & 80% correct in window of 24 trials	at least 250 trials & 75% correct in window of 40 trials	N/A